Adaptive Control Using Constrained RLS and Dynamic Pole-Shift Technique for TCSCs

Dipendra Rai, *Member, IEEE*, Ramakrishna Gokaraju, *Member, IEEE*, and Sherif O. Faried, *Senior Member, IEEE*

***Abstract*—In this paper, an adaptive pole-shift control technique for a FACTS device, namely Thyristor Controlled Series Capacitor (TCSC), is presented. Adaptive pole-shift techniques have been successfully implemented for power system stabilizer applications in the past, but one of the difficulties in extending such a technique for transmission line control devices has been its inability to handle large disturbance conditions such as three-phase faults. In recent literature, random walk technique has been suggested during the system identification process, to overcome this problem. This paper presents a simple parameter constrained RLS identification procedure to track the large disturbance conditions. The effectiveness of the proposed methodology is demonstrated using (*i*) a three-area six-machine power system with a TCSC, and (*ii*) a IEEE 12 bus power system configuration with a TCSC.**

***Index Terms*—Adaptive control, flexible ac transmission systems (FACTS).**

I. Introduction

IN COMPLEX interconnected systems, lightly damped interarea modes of oscillations may get excited during disturbances leading to an unstable system operation [1]. Flexible ac transmission system (FACTS) placed in transmission lines have been used as a mean to damp such oscillations [2], [3]. The phase lead-lag type of controllers is commonly used for the FACTS devices to improve the damping performance. However proper design of the phase lead-lag controllers for FACTS could be a cumbersome task and the difficulties in tuning will be briefly discussed.

One of the presently practiced procedures is to use linearized representation of the FACTS device, and designing the lead-lag controller based on the frequency-response characteristics of the linearized system [4]. Such linearization procedures sometimes hide the unforseen interactions between the different components of the system. The performance of such fixed parameter-based lead-lag controllers is generally good for one or two operating conditions but it has been found that the lead-lag controllers have to be retuned again using analytical tools when the system configuration undergoes significant changes (i.e., when new transmission lines, new types of generation, and power system components are added to the power system).

Manuscript received December 13, 2012; revised May 20, 2013; accepted July 18, 2013. Date of publication September 16, 2013; date of current version January 21, 2014. Paper no. TPWRD-01358-2012.

D. Rai is with BC Hydro, Vancouver, BC V4N 4X8 Canada.

R. Gokaraju and S. O. Faried are with the University of Saskatchewan, Saskatoon, SK S7N 5A9 Canada (e-mail: (e-mail: rama.krishna@usask.ca; sherif.faried@usask.ca).

Color versions of one or more of the figures in this paper are available online at http://ieeexplore.ieee.org.

Digital Object Identifier 10.1109/TPWRD.2013.2279539

Another commonly used procedure for tuning the lead-lag control parameters is using transient simulation programs, which requires a large number of repeated runs of the program. The Monte-Carlo search is one such approach, in which the control parameters are varied in a random manner [5]. This procedure requires a enormously large number of electromagnetic simulation runs.

One recent innovation is using a nonlinear optimization procedure (such as simplex optimization) to reduce the number of electromagnetic simulations runs to find the optimum set of parameters by directing the search to the most promising regions in the search space [6]. However, the controllers optimized offline using such a procedure cannot account for unforeseen significant changes in the system.

Adaptive control techniques do not need such tuning and are able to achieve optimal operation for large disturbance conditions, a wide range of operating scenarios, and significant changes in the system [7]–[9]. The adaptive algorithm works on an estimated plant model at every sampling instant. The adaptive controllers also track the system changes and are able to self-optimize. The model estimator tracks the changes in the power system rapidly and smoothly for uniform control action [10]. In adaptive control, methods based on least-squares filters, such as recursive least squares (RLS) and Kalman filters, are most commonly used for system identification because of their simplicity and numerical stability[11]. However, during large disturbances, parameter identification using least-squares procedures is a real challenge. The parameters identified during such conditions have large and rapid fluctuations [12], and this results in undesirable control output (bang-bang-type control).

The adaptive pole-shift control for FACTS devices have been studied in recent literature [13]–[15]. It was reported in [13] that the start of the estimation process gave poor system response to initial transients while using the recursive least square (RLS) estimator. Similarly, [15] reported that the variable forgetting factor-based RLS results in large variations in estimated parameters during transients leading to wide variations in the control output and poor controller performance.

For better parameter tracking, Sadikovic *et al.* [14], [16] proposed the use of a regularized constant tracing algorithm [10] to keep the correlation matrix symmetrical during the Kalman filter identification procedure. The main aim behind it is to ensure that the covariance matrix stays bounded. Plant dynamics is approximated by a 12th- order autoregressive external input (ARX) model. The authors use a 12th-order autoregressive external input (ARX) plant model and sensitivity approach to modify the pole-shift factor every sampling instant. They use the derivative of control output [17] with respect to

pole-shift factor (sensitivity) to modify the pole-shift factor in each sampling time. Reference [15] proposes a random-walk term for updating the covariance matrix in the RLS algorithm for prespecified duration following a large disturbance to achieve smoother variations in the identified coefficients. The authors implemented a controller dead-zone following large disturbances to give sufficient time for the estimated parameters to settle down. Furthermore, the authors use a 10th-order ARMA model for plant and a fixed pole-shift factor (similar to pole-placement methods) to generate the control signal [7]. This method adds a semi-positive definite matrix to the covariance matrix to hold the trace of the covariance matrix at a constant level for a prespecified duration following disturbance. The control signal is then generated by moving poles to a fixed location (similar to pole-placement methods) using a fixed pole-shift factor [7]. The authors use a 10th-order ARMA model to approximate the power system.

For adaptive control algorithms, computational time is very important. The computational time depends on the order of the discrete model approximation. Obviously, using a higher order model means more calculations for the identifier and the controller. Therefore, it is preferable to use a reduced-order model, which can capture the essential dynamics. Determining an accurate control signal is basically the job of the controller and, hence, generating optimum control evaluations is left to the controller.

In this paper, a simple third-order ARMA model is proposed for the identifier. Any dynamic system that depicts an oscillatory response of one frequency can be modeled as a third-order ARMA model [8]. For a system exhibiting oscillatory behavior, a third-order model is going to have three roots: a pair of complex conjugate roots and a real root. The complex roots represent the oscillatory part and the real root represents the decaying part of the response. For controlling the dominant mode of interarea oscillation in a tie line, a third-order ARMA model was found to be sufficient. It should be noted that there may be other interarea modes of oscillations present, along with the dominant mode, but these nondominant oscillations can be treated as a noise term [17].

This paper also proposes the use of a constrained identification procedure during large disturbance scenarios. The method is simple and involves only a minor calculation step. This method helps in smoothing out the parameter variations effectively during major disturbances and, thus, produces a stable control response.

The contributions of this paper are summarized as follows: 1) A simple constrained identification procedure to prevent large excursions in the parameters during large disturbance conditions. It is worth noting here that the previous literature cited the inability of adaptive control techniques (pole-placement or pole-shift-type controllers) to handle large fault conditions because of the rapid parameter variations during such disturbances; and 2) A dynamic pole-shift method to find the optimum pole locations without excessive control calculations. The previous pole-shift methods for FACTS use control margins-type calculations [7], [14] or use dynamic pole-assignment methods to find the pole locations, but it was found, in the course of this paper, that these simplifications are not necessary, and the minimum variance principle could be used for finding the pole-shift factor efficiently.

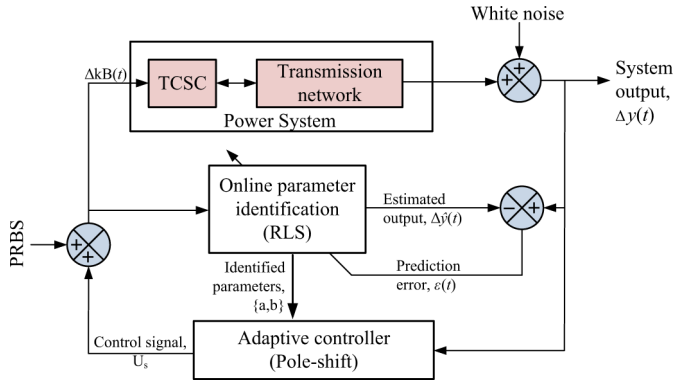

Fig. 1. Indirect adaptive control schematic.

This paper is organized as follows: Section II gives a brief description of the proposed adaptive control technique. The study system is presented in Section III. Section IV describes the TCSC control methodology; and the electromagnetic transient simulation results are reported in Section V. In Section VI, conclusions are presented.

II. Indirect Adaptive Control

The basic concept of the indirect adaptive control scheme for the TCSC is shown in Fig. 1. The white noise term is used to represent unmodelled dynamics. The pseudorandom binary sequence (PRBS) noise is used to excite the plant [10]. The response of the nonlinear power system, including the FACTS device, is modeled by a mathematical model. This type of model is basically a reduced-order or coarse model. The coefficients of the model of the plant are then estimated in real time using a recursive algorithm. The estimated parameters are then used to design an optimum controller to meet the specific control requirements. Once the optimized controller parameters are achieved, the controller generates an appropriate control signal.

The power system dynamics is approximated by a discrete ARMA model of the form [8], [9]

$$A(z^{-1})y(t) = z^{-n_d}B(z^{-1})u(t) + C(z^{-1})e(t) \qquad (1)$$

where $y(t)$, $u(t)$, and $e(t)$ are system output, system input, and noise terms, respectively. $A(z^{-1})$, $B(z^{-1})$, and $C(z^{-1})$ are the polynomials expressed in terms of the backward shift operator z^{-1} and are defined as

$$\begin{aligned} A(z^{-1}) &= 1 + a_1 z^{-1} + a_2 z^{-2} + \cdots + a_{n_a} z^{-n_a} \\ B(z^{-1}) &= 1 + b_1 z^{-1} + b_2 z^{-2} + \cdots + b_{n_b} z^{-n_b} \\ C(z^{-1}) &= 1 + c_1 z^{-1} + c_2 z^{-2} + \cdots + c_{n_c} z^{-n_c}. \end{aligned}$$

n_a, n_b, and n_c are the order of the polynomials $A(z^{-1})$, $B(z^{-1})$, and $C(z^{-1})$, respectively. The variable n_d represents the delay term.

A. Model Estimation

It is desirable to have smooth parameter estimates for large disturbances (faults in the power system). A constrained recur-

sive least square (RLS) algorithm [18] has been proposed in this paper. References [9] and [18] used the constrained RLS algorithm for power system stabilizer applications to minimize the control output variations due to small noise 2% (perturbations) present in the system continuously in the system. This paper addresses an opposite issue to curtail the RLS parameter variations due to large disturbance conditions in power systems (fault conditions) using the constrained RLS procedure for TCSCs. For small disturbances, the constrained RLS just works like a normal RLS algorithm. Since $e(t)$ cannot be directly measured, the regression model of (1) can be obtained by a suitable approximation as [10]

$$y(t) = \Psi^T(t)\theta + e(t) \tag{2}$$

where $\Psi(t)$ is the measurement variable vector

$$\Psi(t) = [-y(t-1)..-y(t-n_a)u(t-n_d). \\ u(t-n_d-n_a)\epsilon(t-1)..\epsilon(t-n_c)]^T. \tag{3}$$

θ is the parameter weight vector

$$\theta = [\, a_1 \quad .. \quad a_{n_a} \quad b_1 \quad .. \quad b_{n_b} \quad c_1 \quad .. \quad c_{n_c}\,]^T \tag{4}$$

and

$$\epsilon(t) = y(t) - \Psi(t)\hat{\theta}(t-1) \tag{5}$$

is the estimation error. Here, the variable $e(t)$ is approximated by the estimation error $\epsilon(t)$.

The system parameter weight vector $\theta(t)$ can be estimated using the following extended RLS equations algorithm [10]:

$$\hat{\theta}(t) = \hat{\theta}(t-1) + K(t)\left[y(t) - \Psi(t)^T\hat{\theta}(t-1)\right] \tag{6a}$$

$$K(t) = \frac{P(t-1)\Psi(t)}{\lambda(t) - \Psi(t)^T P(t-1)\Psi(t)} \tag{6b}$$

$$P(t) = \frac{1}{\lambda(t)}\left[P(t-1) - K(t)\Psi^T(t)P(t-1)\right] \tag{6c}$$

where $\lambda(t)$ is the time-varying forgetting factor, $P(t)$ is the covariance matrix, and $K(t)$ is the gain vector. As discussed before, during large disturbances, the identified plant parameters vary significantly. To limit such large deviations in parameters, a simple constraint term $\beta(t)$ is introduced in the update algorithm equation (6a)–(c) as given

$$\hat{\theta}(t) = \hat{\theta}(t-1) + K(t)\left[y(t) - \Psi(t)^T\hat{\theta}(t-1)\right]\beta(t) \tag{7}$$

where $\beta(t)$ is calculated in each sampling time interval as follows:

$$\beta(t) = \begin{cases} 1.0 & \text{if} \frac{N_2}{N_1} \le \beta_0 \\ \frac{\beta_0}{N_2} & \text{if} \frac{N_2}{N_1} > \beta_0 \end{cases} \tag{8}$$

where

$$N_1 = \|\hat{\theta}(t)\|_2 \\ N_2 = \|K(t)[y(t) - \Psi(t)^T\hat{\theta}(t)]\|_2.$$

$\|.\|_2$ is the norm of the corresponding vector, and β_0 is a positive constant. $\beta_0 = 0.10$ is selected to switch on the constrained least squares identification procedure for disturbances greater than 10%.

The $\beta(t)$ term in (7) keeps the parameter vector $(\hat{\theta}(t))$ and the covariance matrix $(P(t))$ bounded during a large disturbance condition.

B. Pole-Shift Control

Once the parameters of the model are properly estimated, an optimized pole placement controller, (known as the pole-shift controller [9]), is designed to generate the optimal control signal. The proposed controller combines the principle of the minimum variance control (minimizes the deviation of the plant output with desired output) and the pole-assignment control principle (assigns the closed-loop poles to predefined locations with the unit circle in the z-plane). The transfer function is of the form:

$$\frac{u(t)}{y(t)} = -\frac{G(z^{-1})}{F(z^{-1})} \tag{9}$$

where

$$F(z^{-1}) = 1 + f_1 z^{-1} + f_{-2}z^{-2} + \cdots + f_{n_f}z^{-n_f} \\ G(z^{-1}) = g_0 + g_1 z^{-1} + g_2 z^{-2} + \cdots + g_{n_g}z^{n_g}$$

and $n_f = n_b - 1$, $n_g = n_a - 1$. From (1) and(20), the characteristic equation can be derived as follows:

$$T(z^{-1}) = A(z^{-1})F(z^{-1}) + B(z^{-1})G(z^{-1}). \tag{10}$$

If the characteristic polynomial $T(z^{-1})$ is predefined as in pole-assignment control, the controller polynomials $F(z^{-1})$ and $G(z^{-1})$ can be calculated from (10). However, in pole-shift control, the characteristics equation of (10) takes the form of $A(z^{-1})$ with the pole shifted by a factor of α. The new characteristics equation can be obtained by replacing z^{-1} in $A(z^{-1})$ by αz^{-1} as follows:

$$A(\alpha z^{-1}) = T(z^{-1}) = A(z^{-1})F(z^{-1}) + B(z^{-1})G(z^{-1}). \tag{11}$$

By forcing the polynomial $T(z^{-1})$ to take the form $A(\alpha z^{-1})$, the control signal $u(t)$ is also made to be a stable signal.

Equation (11) can be rearranged in a matrix form

$$Mw(\alpha) = L(\alpha) \tag{12}$$

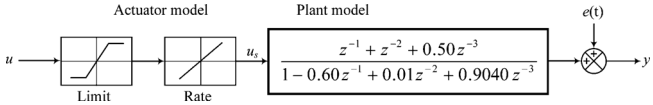

Fig. 2. Nonlinear third-order discrete system.

where

$$M = \begin{bmatrix} 1 & 0 & . & 0 & b_1 & 0 & . & 0 \\ a_1 & 1 & . & 0 & b_2 & b_1 & . & 0 \\ . & a_1 & . & . & . & b_2 & . & . \\ a_{n_a} & . & . & 1 & b_{n_b} & . & . & b_1 \\ 0 & a_{n_a} & . & a_1 & 0 & b_{n_b} & . & b_2 \\ . & 0 & . & . & . & 0 & . & . \\ . & . & . & . & . & . & . & . \\ 0 & 0 & . & a_{n_a} & 0 & 0 & . & b_{n_b} \end{bmatrix}$$

$w(\alpha) = \begin{bmatrix} f_1 & f_2 & .. & f_{n_f} & g_0 & g_1 & .. & g_{n_g} \end{bmatrix}^T$, and $L(\alpha) = [a_1(\alpha_t - 1)\ a_2(\alpha_t^2 - 1)\ ..\ a_{n_a}(\alpha_t^{n_a} - 1)\ 0\ ..\ 0\ 0]^T$. and α_t is the pole-shift factor at time t.

a_i and b_i are identified at every sampling instant. Equation (12) can be solved for f_i and g_i for a known value of α. Once the values of f_i and g_i are obtained, the control signal can be computed using (20). It can be observed that the control signal is a function of α at any time t, let us say α_t. The control signal $u(t, \alpha_t)$, can be expressed in a Taylor series in terms of factor α_t around an operating point α_0 as

$$u(t, \alpha_t) = u(t, \alpha_0) + \sum_{i=1}^{\infty} \frac{1}{i!} \left[\frac{\partial^{(i)} u(t, \alpha_t)}{\partial \alpha_t^{(i)}} \right] (\alpha_t - \alpha_0)^i. \quad (13)$$

Substituting (13) into (9), and using(12), the control signal can be expressed as

$$u(t, \alpha_t) = X^T(t) w(\alpha_t) = X^T(t) M^{-1} L(\alpha_t) \quad (14)$$

where $X(t) = [-u(t-1)..-u(t-n_f) - y(t) - y(t-1)..y(t-n_g)]^T$ is the measurement variable vector. The ith-order differential of $u(t, \alpha_t)$ with respect to α_t becomes

$$\left[\frac{\partial^{(i)} u(t, \alpha_t)}{\partial \alpha_t^{(i)}} \right]_{\alpha_t = \alpha_0} = X^T(t) M^{-1} L^{(i)}(\alpha_0) \quad (15)$$

where i represents the order of differentiation. Now, (13) can be written in a simple form as

$$u(t, \alpha_t) = u(t, \alpha_0) + \sum_{i=1}^{n_a} s_i \alpha_t^i \quad (16)$$

where

$$s_i = \frac{1}{i!} X^T(t) M^{-1} L^{(i)}(\alpha_0).$$

Once the input is computed at time t, the system-predicted output $\hat{y}(t+1)$ at time $t+1$ can be calculated as follows:

$$\hat{y}(t+1) = X^T(t)\beta + b_1 u(t, \alpha_t) \quad (17)$$

where

$$\beta = [\, -b_2 \quad -b_3 \quad \ldots \quad -b_{n_b} \quad a_1 \quad a_2 \quad \ldots \quad a_{n_a} \,]$$

is an identified parameter vector. For a fixed value of α_t, control becomes a special case of the pole-assignment control. The value of α_t is obtained using the minimization of the one time-step ahead system output prediction error cost function given

$$\min_{\alpha_t} J(t+1, \alpha_t) = E\left[\hat{y}(t+1) - y_r(t+1)\right]^2 + \mu(\alpha_t - \alpha_{ss})^2 \quad (18)$$

where $y_r(t+1)$ is the reference output for the next time step, μ is a weighting coefficient, and α_{ss} is the steady-state pole-shift factor. By minimizing the performance index of (18), the controlled system output $y(t)$ follows the prespecified reference $y_r(t)$ as close as possible. Minimization of the objective function defined in (18) yields the optimal value of α_t. The value of α_t should be kept in the range of $[-1/\lambda_t < \alpha_t < 1/\lambda_t]$ to satisfy the stability constraints, where λ_t represents the largest absolute value of the roots of characteristics equation $T(z^{-1})$. Furthermore, the control signal also should lie within the control constrain: $u_{\min} \le u(t, \alpha_t) \le u_{\max}$, where $u_{\min}$ and $u_{\max}$ are minimum and maximum control signal boundaries. Equation (18) is a 6th-order polynomial and the Nelder–Mead simplex method is used to find the minimum point in a few iterations (< 7).

C. Nonlinear Third-Order Discrete System Example

A nonlinear third-order discrete system, as shown in Fig. 2, has been used first for the testing of an adaptive pole-shift algorithm. The plant is an *unstable* third-order model with actuator dynamics. The actuator includes a saturation limit and a slew rate limit. The actuator saturation limit cuts off input values greater than $0.55\ units$ or less than $-0.55\ units$. The slew rate limit of the actuator is 0.8 units/s.

The $e(t)$ term represents white noise of 1% magnitude. The open loop poles of the plant are -0.8, and $0.7 \pm j0.8$. Complex conjugate poles of an open-loop system are located outside the unit circle. The system coefficients are identified using the constrained RLS algorithm presented in (6). The control signal is calculated using (16) so that the cost function given in (18) is minimized.

The system time response to the square-wave reference waveform of magnitude ± 1 is plotted in Fig. 3. As seen in Fig. 3(a), the controlled plant is able to track the reference signal effectively. Furthermore, the constrained RLS identification algorithm is able to identify plant coefficients effectively as shown in Fig. 3(b)–(d). Due to the nonlinear nature of the plant, identified coefficients are optimal values rather than actual values. The identified coefficient variations are smooth even for large step changes in the reference waveform: -1 to $+1$ or $+1$ to -1. The effect of actuator dynamics on the control signal is demonstrated in Fig. 3(c). The control signal is rate-limited and clipped whenever the change in reference signal occurs. This introduces nonlinearity on the system.

The dynamic location of open- and closed-loop poles of the system at $t = 53.8$ s is plotted inFig. 4(a). Open-loop poles are shown in the *thin line* and closed-loop poles are shown in

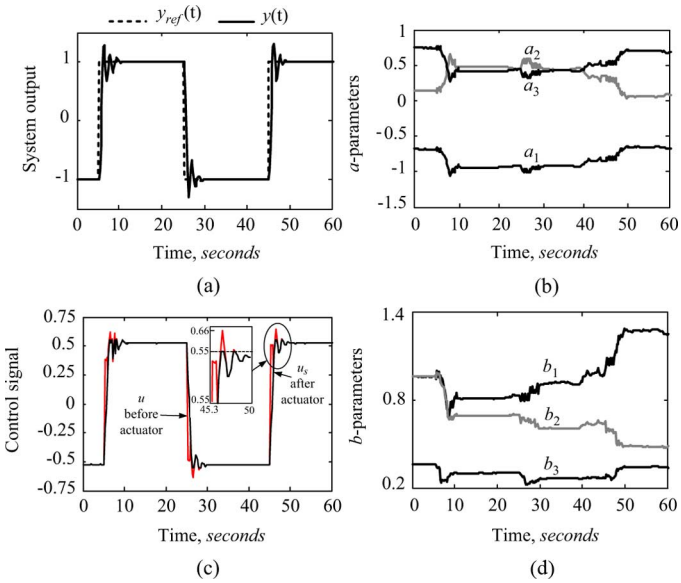

Fig. 3. Nonlinear system response to step change in the reference signal. (a) Reference and output. (b) Numerator coefficients. (c) Control signal saturation and rate limit. (d) Denominator coefficients.

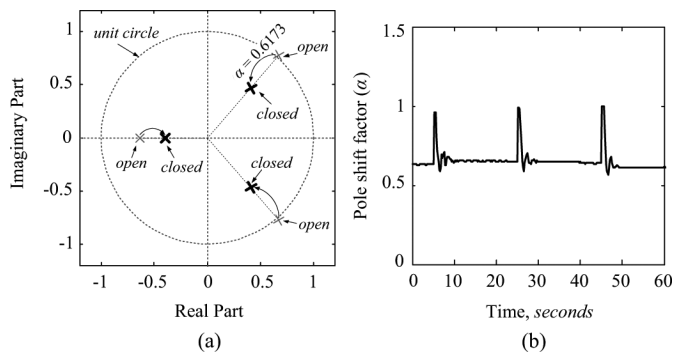

Fig. 4. Dynamic-pole movement with respect to the pole-shift factor α. (a) Dynamic-pole movement. (b) Optimal pole-shift factor.

the *thick line*. The identified open-loop poles are $\{-0.7027, 0.6811 \pm j0.7807\}$, Closed-loop poles are $\{-0.4338, 0.4205 \pm j0.4819\}$, and the pole-shift factor is $\alpha = 0.6173$. The controller transfer function at $t = 53.8$ s is

$$\frac{u(t)}{y(t)} = \frac{0.2755 - 0.2633z^{-1} - 0.5819z^{-2}}{1 + 0.5443z^{-1} + 0.2585z^{-2}.} \qquad (19)$$

It is evident from Fig. 4 that the pole-shift controller improves the stability of the system by moving the poles outside the unit circle to inside the unit circle. The optimal pole-shift factor is plotted in Fig. 4(b)

III. Test Systems

The first test system considered is a three-area, six-machine system as shown in Fig. 5. The 400-km transmission line between buses 7 and 9 is series compensated using capacitor banks and TCSC combination. The compensation degree is defined as the ratio $((X_C + X_{\mathrm{TCSC}})/X_L) \times 100\%$, where X_L is the line inductance, and X_C and X_{TCSC} are the fixed capacitor and TCSC capacitive reactances, respectively. Shunt capacitors are

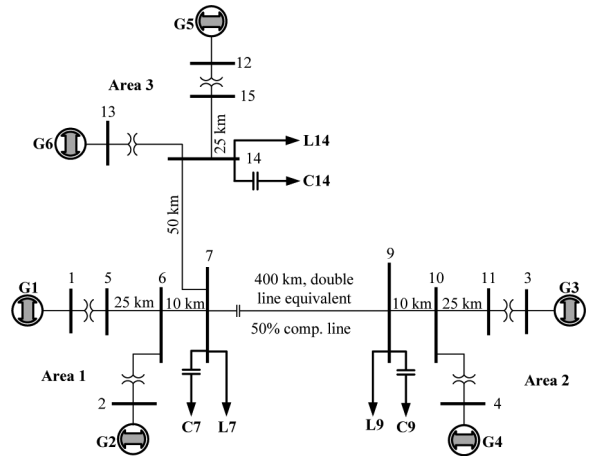

Fig. 5. Schematic diagram of the three-area test system.

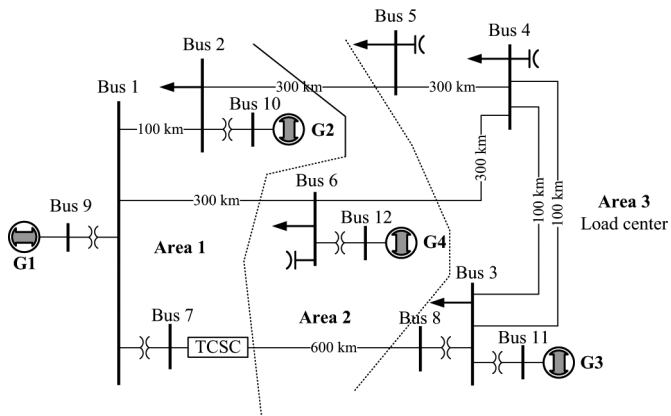

Fig. 6. Modified IEEE 12-bus test system.

installed at buses 7, 9, and 14 to maintain the initial bus voltage profiles within 1 ± 0.03 p.u. The electromagnetic transient simulation software PSCAD/EMTDC is used for simulations. The synchronous generators are represented in the $d-q-0$ reference frame using 7th-order differential equations [19]. The complete TCSC model described in [20] is used in the simulation studies. The machines, and the TCSC data are given in the Appendix.

The rotor angle oscillation modes for the three-area test system are obtained using the eigenvalue analysis. The results are given in Table I. There are five different modes of oscillations: three local modes in each area, and two interarea modes. Interarea Mode 1 is characterized by having a slightly higher frequency ($(0.78Hz)$) than Mode 2 ($(0.46Hz)$). The inter-area oscillations mode shapes are shown in Fig. 7.

For further verification of the proposed adaptive controller, a modified 12 bus test power system reported in [21] (the system is being standardized as an IEEE test system), as shown in Fig. 6 is used. The system has three areas: area 1 is mainly generation, area 3 is load center and area 2 has one generator. This system is large enough to demonstrate electromechanical oscillation modes, and, reasonably sized for doing detailed electromagnetic transient simulation studies. The system exhibits three lightly damped interarea modes of oscillation which are closely spaced: 1.12 Hz, 0.85 Hz, and 0.75 Hz, respectively. The oscillation modes have damping factors of 3.30%, 1.07%, and 7.17%,

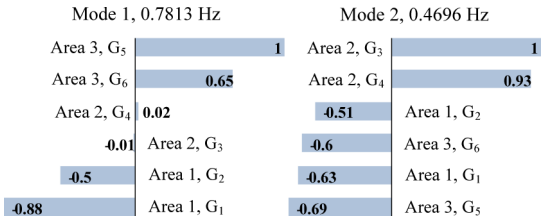

Fig. 7. Mode shapes of the three-area test system.

TABLE I
ROTOR ANGLE MODES OF THE THREE-AREA TEST SYSTEM

Mode type	Real part (σ)	Imaginary part (ω_d)	Frequency (Hz)	Damping ratio ($\zeta, \%$)
Local	-0.5840	7.6616	1.2194	7.60
	-0.5767	6.8333	1.0876	8.41
	-0.7099	6.6681	1.0613	10.59
Inter-area	-0.1730	4.9093	**0.7813**	3.52
	-0.8353	2.9503	**0.4696**	27.24

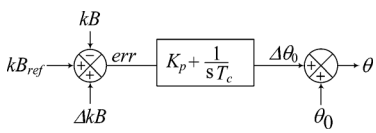

Fig. 8. TCSC control.

respectively, which are very close to each other. The eigenvalue analysis and more detailed description of the system could be found in [21].

The generators G_2 and G_3 are hydro generators and generator G_4 is a thermal generator. The generators are modelled using $7th$ order differential equations [19]. The constant voltage and frequency source model G_1 at infinite bus in [21] is replaced by a classical generator with finite inertia of $20s$.

IV. INTERAREA OSCILLATION DAMPING USING TCSC

The real power flow in a transmission line is proportional to the inverse of the total line reactance, and therefore, the power swing damping can be achieved by properly modulating the TCSC impedance [22]. A supplementary controller can be used for obtaining the proper impedance modulation. In the proposed work, proper modulation of TCSC impedance is achieved using an adaptive supplementary controller described in Section II.

The proportional-integral-type controller is used to control steady state TCSC impedance at a desired level, as shown in Fig. 8. $kB_{\rm ref}$ is the TCSC boost level set point and ΔkB is the supplementary control signal for power swing damping. The boost factor/level is the ratio of the apparent reactance of the TCSC seen from the line to the physical reactance of the TCSC capacitor bank at fundamental frequency. Positive value of boost factor is assumed for capacitive impedance, and negative value for inductive impedance. In this study, only the capacitive operating region (positive boost factor) is considered. θ is the thyristor firing angle, and θ_0 is the initial firing angle.

The supplemental controller input (stabilizing) signals could be local (e.g., real power flows) or remote (e.g., load angles or speed deviations of remote generators). Local signals are used for the reasons of simplicity and the ease of measurement. The available local signals are studied using Prony analysis to select the proper inputs to the supplementary controller. The Prony analysis decomposes a signal into a series of damped complex exponentials or sinusoids, and therefore, is very helpful in identifying the most dominant modes of oscillations present in a signal [23]. The Prony analysis of the rotor angle oscillations of the generators in area 2 (Fig. 5) reveals that the generators mainly participate in Mode 2 oscillation, as indicated by mode shapes of the system (Fig. 7). Furthermore, Prony analysis of power flow through tie-line between buses 7–9 reveals that Mode 2 of the interarea of oscillation is present. Since placement of TCSC on tie-line 7–9 has direct impact on the interarea oscillation between area 2 and area 1 or area 2 and area 3, the local input to the supplemental controller is chosen as the tie-line power flows of buses 7–9.

1) Conventional Lead-lag Supplementary Controller: The time constants and gain of the controller are optimized using multiple time-domain simulation-based simplex algorithm. This tuning procedure is currently being used by the industry for tuning of the controller parameters [6].

V. SIMULATION STUDIES

A. TCSC-Compensated Three-Area Power System (Fig. 5)

The TCSC is assumed to be installed in the test system (Fig. 5) between buses 7 and 9, replacing the portion of fixed series capacitive compensation of both lines. The total series compensation is 0.5 p.u. of the total line reactance, and the TCSC contribution in the total compensation is 0.25 p.u. The deviation in power flow through line 7–9 is considered as plant output. The supplementary control signal ΔkB is considered as plant input. The reference $y_r(t+1)$ in (18) is set to zero.

The study system has the highest interarea mode of oscillation of 0.7813 Hz. So a sampling frequency of 10 Hz for the identifier and controller is found to be sufficient. Furthermore, the extended recursive least square identification method given in (6) was able to find the plant coefficients effectively by including the 2nd-order noise terms. The Nelder–Mead simplex optimization algorithm is used for the minimization of the cost function. The maximum number of iterations for optimization was found to be less than 7 for all the test scenarios presented in this paper. The modern computing hardware need a very small fraction of the total sampling time for this kind of optimization. An Intel Visual FORTRAN program code was developed and interfaced to the PSCAD/EMTDC tool. The program subroutine takes samples of plant output and generates the pole-shift control signal to the plant.

Different system contingencies listed in Table II, were studied in order to evaluate the effectiveness of the control. System loading for the study cases are given in Table III. The disturbances are applied at 1 s for $3cycles$. The simplex optimization procedure took 150 simulation runs to optimize parameters T_1, T_2, T_3, T_4, and K_p for disturbance A and the values obtained are reported in the Appendix.

The performance of the parameter constrained RLS estimation algorithm is shown in Fig. 9.Fig. 9(a) shows the identified

TABLE II
INTERAREA OSCILLATION DAMPING CASE STUDIES

Approximate power flow on line 7-9	Disturbance description	Disturbance type
415 MW	3-phase-to-ground fault (bus 7)	***A***
415 MW	2-phase-to-ground (a,b -ground) fault (bus 7)	***B***
220 MW	3-phase-to-ground fault (bus 7)	***C***
-180 MW	3-phase-to-ground fault (bus 7)	***D***
415 MW	300 MW load rejection (bus 9)	***E***

TABLE III
LOAD DATA (MVA, MVAR) FOR DIFFERENT CASE STUDIES.

Case	Bus 7 (L_7, C_7)	Bus 9 (L_9, C_9)	Bus 14 (L_{14}, C_{14})
A, *B*, *E*	$1400 + j100$, $-j350$	$1800 + j100$, $-j500$	$1200 + j100$, $-j220$
C	$1400 + j100$, $-j260$	$1600 + j100$, $-j350$	$1450 + j100$, $-j220$
D	$1755 + j100$, $-j260$	$1200 + j100$, $-j350$	$1200 + j100$, $-j240$

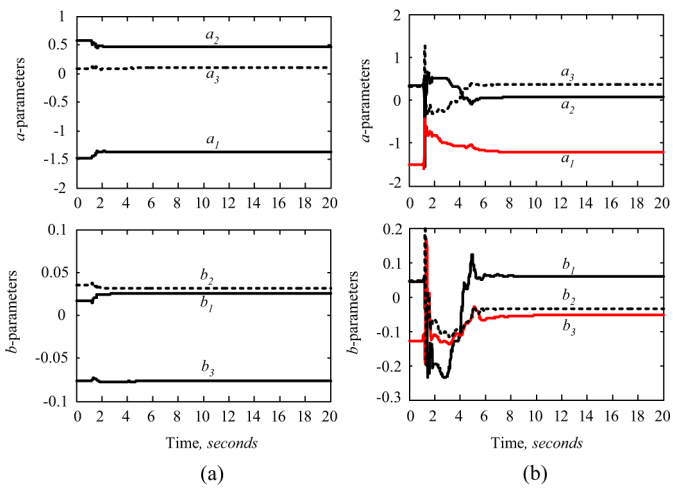

Fig. 9. Parameter identification using RLS technique for the disturbance *A*. (a) Parameter constrained RLS (b) Nonconstrained RLS.

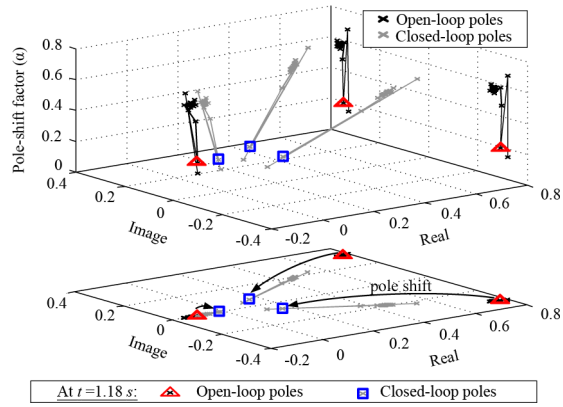

Fig. 10. Dynamic poles movement as a function of pole-shift factor α for the disturbance*A*.

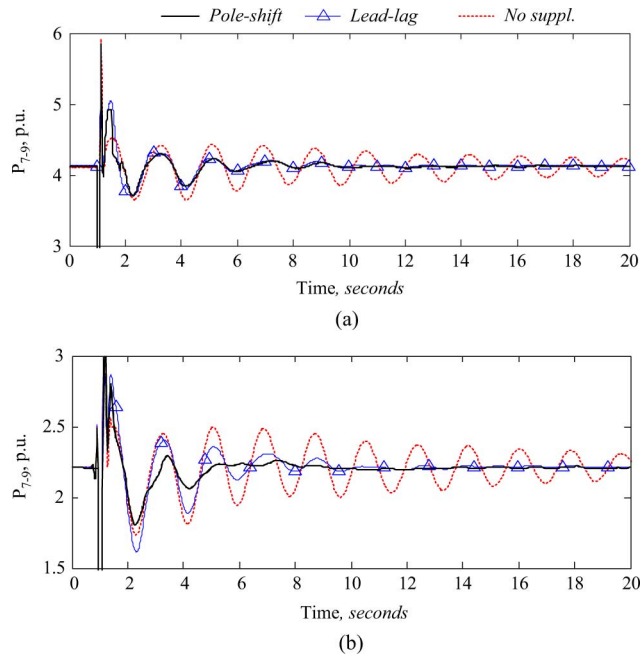

Fig. 11. Tie-line power flows for the disturbances. (a) Disturbance*A* ; (b) Disturbance *C*.

plant parameters using the parameter constrained RLS algorithm for the disturbance *A*. It is evident that the proposed constrained identification method helps to identify the system parameters smoothly even during a large disturbance. On the other hand, Fig. 9(b) shows the estimated plant parameters for the same case study of Fig. 9(a), using the nonconstrained RLS algorithm, and from the results, it can be seen that a large change in parameter values occur during the disturbance. This sudden change in parameter values cause an undesirable controller output, which leads to a poorly damped performance.

Fig. 10 shows the dynamic pole-shifting process for the case study of Fig. 9(a). The closed-loop poles and open-loop poles are captured for the duration of 1 to 4.4 s and plotted as a function of pole-shift factor α. The closed-loop and open-loop poles of the system at time $t = 1.18$ s are indicated by a triangle (*open loop*) and a square (*closed loop*) and, at this time, the pole-shift factor is $\alpha = 0.149$. It can be observed from the result that during the transients, there is a significant amount of pole-shifting taking place. The controller generates optimal control signal by moving poles closer to the origin. The steady state pole-shift factor for this case is found to be $\alpha = 0.5952$ and identified plant coefficients are $a = [-1.374, 0.457, 0.096]$ and $b = [0.025, 0.031 - 0.076]$, respectively. Using (11), the transfer function of the controller can be derived as

$$\frac{u(t)}{y(t)} = \frac{3.501 - 4.614z^{-1} - 0.738z^{-2}}{1 + 0.644z^{-1} + 0.585z^{-2}}. \tag{20}$$

The effectiveness of the proposed control algorithm for damping interarea oscillations is demonstrated in Figs. 11–16. Fig. 11 shows tie-line power flow (line 7–9) for disturbances*A* and*C*Fig. 11(a)- Fig. 11(b)show that the pole-shift supplementary controller effectively damps the tie-line power oscillations compared to the traditional lead-lag controller. The identified plant parameters and dynamic pole movement, with respect to pole-shift factor for the cases of Fig. 11(a), are shown in Fig. 9(a) and 10, respectively. Furthermore,Fig. 12(a) shows

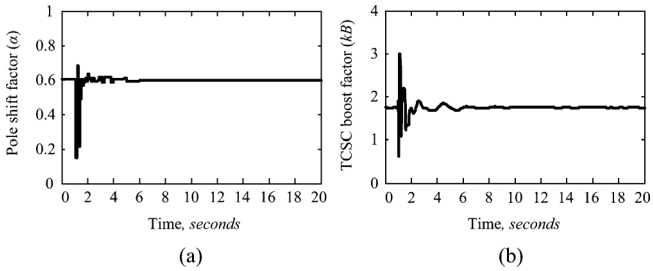

Fig. 12. Pole-shift factor and TCSC boost factor variations for the disturbance A. (a) Pole-shift factor α; (b) TCSC boost factor kB.

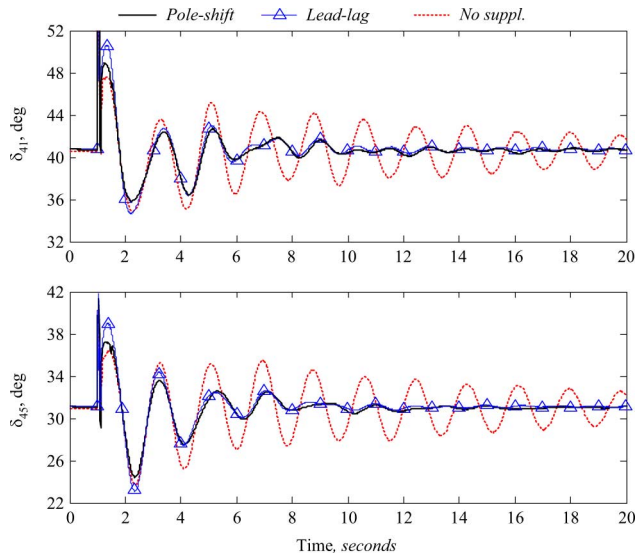

Fig. 13. Generators G_1 and G_5 load angle, measured with respect to G_4 load angle for the disturbance$A$.

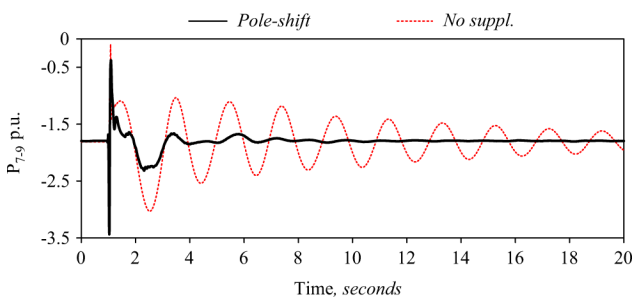

Fig. 14. Tie-line power flow for the disturbance$D$.

the pole-shift factor, and Fig. 12(b) shows the TCSC boost factor for the case study used for Fig. 11(a).

The generator G_1 (area 1) and G_5 (area 3) load angles, measured with respect to G_4 (area 2) load angle for disturbance$A$ is shown in Fig. 13. It is evident from the results that the supplementary controller helps to damp out the interarea oscillations effectively and faster.

Fig. 14 shows the tie-line (line 7–9) power flow variations for the disturbance D (power flow reversal followed by a three-phase-to-ground fault at bus 7). The power flow reversal introduces 180° phase shift to the input signal, and in this case, the conventional controller would need a separate triggering signal to detect the reversal of power flow so that the phase can be

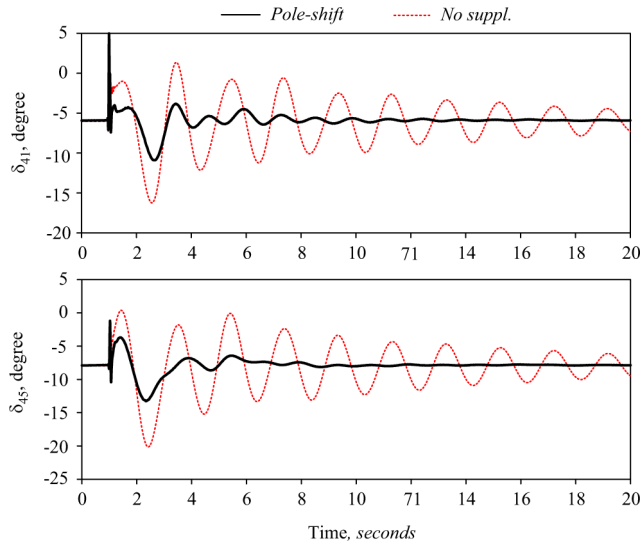

Fig. 15. Generators G_1 and G_5 load angle, measured with respect to G_4 load angle, for the disturbance$D$.

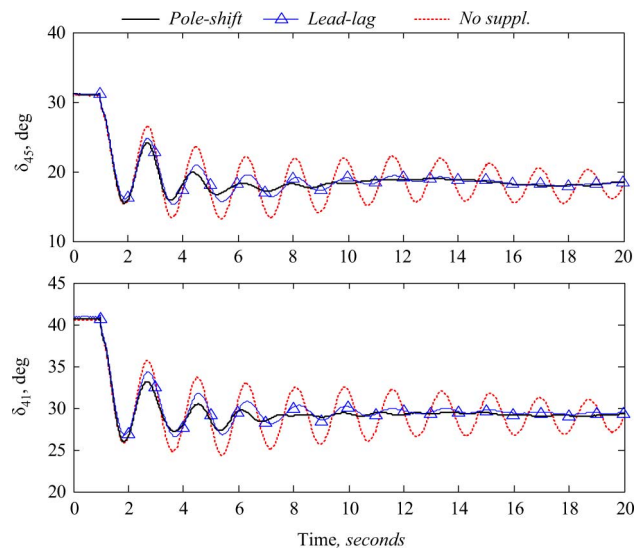

Fig. 16. Generators G_1 and G_5 load angle, measured with respect to G_4 load angle, for the disturbance$E$.

TABLE IV
IEEE 12-BUS TEST SYSTEM STUDIES

Disturbance description	Disturbance type
1-phase-to-ground (a-ground) 200ms fault (bus 3)	***A***
3-phase-to-ground 200ms fault (bus 3 and 6)	***B***
3-phase-to-ground fault at 100km from bus 4 on line 4-5, fault cleared by disconnecting line 4-5 after 9$cycles$	***C***

adjusted to achieve the proper damping. Whereas the proposed adaptive controller, without any external interference, adjusts to a correct set of identified parameters, and generates a stable control behavior.

A significant change of operating point is obtained by disconnecting a 300-MW load at bus 9 at $t = 1$ s (case$E$). The G_1 and G_5 load angles, measured with respect to G_4 load angle,

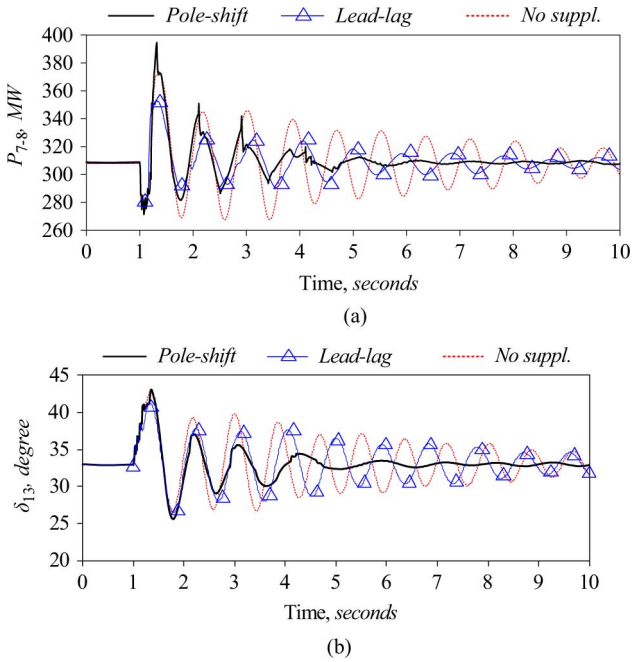

Fig. 17. Line power flow and load angle (G_3 with respect to G_1) variations for the disturbance$A$ (IEEE 12 bus test system). (a) Power flow on line 7–8; (b) Generator rotor angle δ_{1-3}.

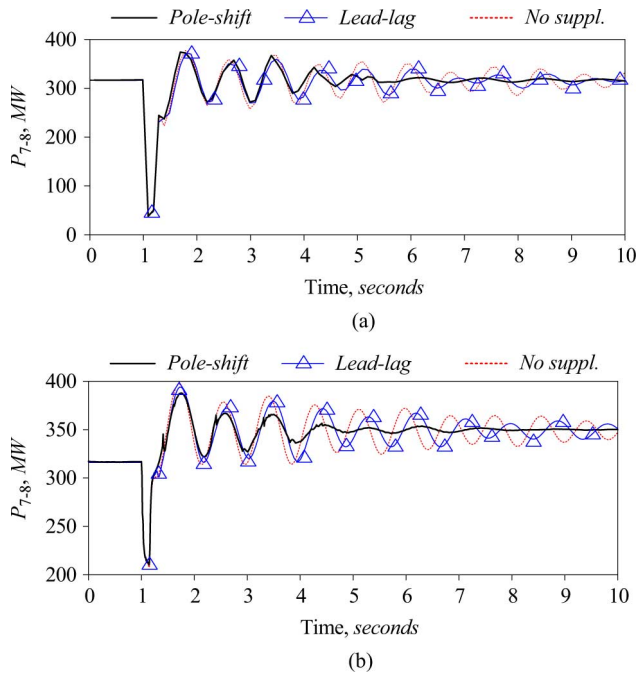

Fig. 18. Line power flow (line 7–8) for the disturbances$B$ and$C$ (IEEE 12 bus test system). (a) Disturbance$B$; (b) Disturbance C.

TABLE V
PRONY ANALYSIS OF POWER FLOW ON LINE L7–8 (DISTURBANCEB)

Modes	No suppl.	Lead-lag	Pole-shift
Mode 1 - f(Hz), Damping (%)	$1.209Hz$, 2.18%	$1.185Hz$, 4.10%	$1.221Hz$, 9.38%
Mode 2 - f(Hz), Damping (%)	$0.891Hz$, 1.32%	$0.901Hz$, 1.81%	$0.870Hz$, 11.69%
Mode 3 - f(Hz), Damping (%)	$0.762Hz$, 4.14%	$0.764Hz$, 5.01%	$0.660Hz$, 32.74%

are shown in Fig. 16. The pole-shift control provides better damping, and faster settling time compared to the lead-lag controller. It should be noted here that the lead-lag controller has been optimized for case A, and its performance deteriorated as operating point changed to a new value. Similar responses were observed for disturbance case B as well.

B. IEEE 12-Bus Test System Studies (Fig. 6)

For the simulation studies, a TCSC unit is placed near bus 7 between line 7–8. The steady-state series capacitive compensation provided by TCSC is 0.15 p.u. of the total line impedance. The power flowing through line 7–8 is taken as input to the supplementary controller [21]. Three test cases are studied as shown in Table IV. The disturbances are applied at $t = 1$ s and responses are plotted for 0- to 10-s time window.

Fig. 17 shows the tie-line power flow through line 7–8 and rotor angle deviation of G_3 with respect to G_1 for the disturbance case$A$. To excite the multi-mode oscillations in case B, 3-phase-to-ground faults are applied at bus 3 and 6 simultaneously and cleared at $200ms$. Fig. 18(a) and (b) shows the tie-line power flow through line 7–8 for more severe disturbance cases$B$ and$C$, respectively. Fig. 19(a) and (b) shows the generator rotor angle deviation of generator G_3 with respect to G_1 for the same

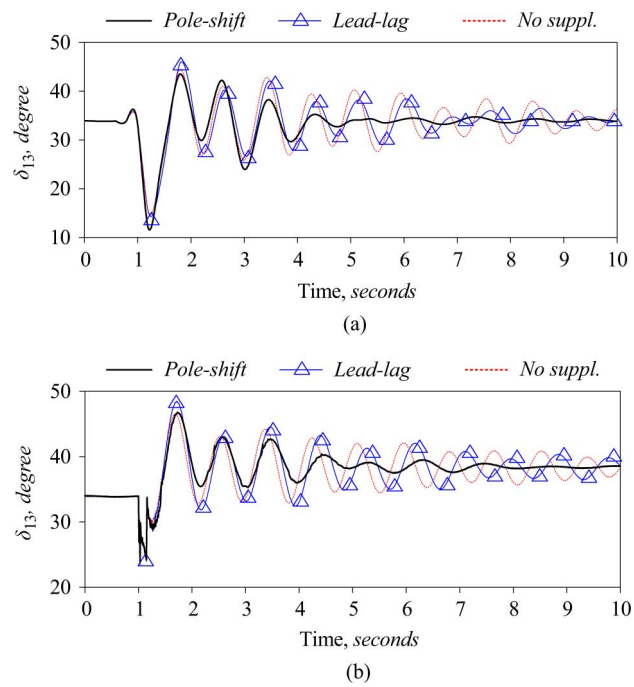

Fig. 19. Generator rotor angle of generator G_3 with respect to G_1 for the disturbances (a)B and (b)C (IEEE 12 bus test system). (a) Disturbance$B$; (b) Disturbance C.

disturbances B and$C$. In all three cases, the proposed controller provides better damping and faster settling time compared to the conventional controller. The lead-lag supplementary controller is tuned for disturbance type B, and, hence, its performance is better for this case and deteriorates for other disturbances, whereas, the operating condition does not affect the performance of the proposed adaptive controller.

The severe disturbances in cases *B* and*C* excites multi-mode oscillations. The Prony analysis on the power flow on line 7–8 for case*B* reveals the presence of three modes as shown in Table V. The approximate damping factors from the Table shows that the pole-shift controller improves the multi-mode oscillation damping. The disturbance case**C** is used to simulate delayed breaker operation ($9\ cycles$) for clearing the faulted line, and, even under such a situation, the proposed algorithm damps the oscillations very effectively. The response also shows that the proposed adaptive controller provides good damping even when the interarea modes are closely spaced.

VI. Conclusion

This paper proposed the use of a simple parameter constrained recursive least square identification technique to handle large disturbances (faults, line switching etc) in adaptive control techniques. The results using a TCSC controller showed that the proposed constrained identifier smoothed out the estimated coefficient variations effectively during large disturbances. The proposed estimation procedure helped in achieving an effective control action using the pole-shift-type controller, and also overcame the problems discussed in the recent literature with regard to applying this technique during the faulted conditions. A phase lead-lag controller provides a good response when optimally tuned. However, this tuning procedure is cumbersome for a TCSC due the complexity of the power-electronic circuits. Whereas, the main advantage of the proposed adaptive controller is that it does not require any tuning for different operating conditions or different power system configurations, and provides better or as good a performance as a well-tuned phase lead-lag controller. In addition, the computations required for the adaptive controller are not extensive. The proposed adaptive control algorithm have been recently implemented on a TI TMS320C6713 floating point DSP board and have recently been verified using real-time digital simulations. The identification routine took $0.10ms$ to execute on the TI board and the pole-shit controller took a maximum time of $0.18ms$ to execute on the TI DSP board. The hardware implementation of the proposed controller and the real-time verification would be reported in a subsequent publication.

Appendix
Machine and System Data

Generator Data: $900MVA$, $20kV$, $r_a = 0.0025$ p.u., $x_l = 0.2$ p.u., $x_d = 1.8$ p.u., $x_q = 1.7$ p.u., $x'_d = 0.3$ p.u., $x'_q = 0.55$ p.u., $x''_d = 0.25$ p.u., $x''_q = 0.25$ p.u., $T_{d0} = 8$ s, $T''_{d0} = 0.03$ s, $T'_{q0} = 0.4$ s, $T''_{q0} = 0.05$ s, $H(G_1\&G_2) = 6.5$ s, $H(G_3\&G_4) = 6.175$ s, $H(G_5) = 5.5$ s, $H(G_6) = 5$ s.

Generator Steady-State Data: G_1: $V = 1.03\angle 0^0$ p.u., G_2: 700 MW, $V = 1.01$ p.u., G_3: 720 MW, $V = 1.01$ p.u., G_4: 700 MW, $V = 1.01$ p.u., G_5: 800 MW, $V = 1.02$ p.u., G_6: 780 MW, $V = 1.01$ p.u.

Transmission Line Data: $r = 0.053\Omega/km$, $X_L = 0.53\Omega/km$

Exciter Data: IEEE-type ST1A exciter, $T_r = 0.01$ s, $T_C = 1$ s, $T_B = 10$ s, $K_A = 50$, V_{MAX} =9 p.u., $V_{MIN} = -9$ p.u.

Steam Governor Data: GE mechanical-hydraulic controls, Droop $(R) = 0.04$ p.u., Speed relay lag time constant (TC) $(T_1) = 0.1$ s, Gate servo TC $(T_3) = 0.25$ s.

Steam Turbine Data (in P.u.): IEEE-type 2 thermal turbine, $K_1 = 0.0$, $K_3 = 0.25$, $K_5 = 0.0$, $K_7 = 0.0$, $K_2 = 0.25$, $K_4 = 0.5$, $K_6 = 0.0$, $K_8 = 0.0$, Steam chest TC $(T_4) = 0.42s$, Reheater TC $(T_5) = 4.25s$, Reheater/cross-over TC $(T_6) = 0.72s$.

TCSC Parameters: $kB_{\rm ref} = 1.75$, $C_{\rm TCSC} = 87.76\mu F$, $L_{\rm TCSC} = 12.8mH$, PI controller: $K_P = 10$, $T_C = 0.05s$.

Simplex-Optimized Lead-lag Supplementary Controller: $T_w = 1s$, $T_1 = T_3 = 0.17072s$, $T_2 = T_4 = 3.2925s$, $K_P = 0.057$.

Acknowledgment

This research work was done at the University of Saskatchewan.

References

[1] M. Klein, G. Rogers, and P. Kundur, "A fundamental study of inter-area oscillations in power systems," *IEEE Trans. Power Syst.*, vol. 6, no. 3, pp. 914–921, Aug. 1991.

[2] P. Pourbeik and M. J. Gibbard, "Damping and synchronizing torques induced on generators by facts stabilizers in multimachine power syst," *IEEE Trans. Power Syst.*, vol. 11, no. 4, pp. 1920–1925, Nov. 1996.

[3] C. Gama, L.Ångquist, G. Ingeström, and M. Noroozian, "Commissioning and operative experience of TCSC for damping power oscillation in the Brazilian north-south interconnection," *CIGRÉ rue d'Artois F-75008 Paris*, vol. 21, no. 14-104, 2000.

[4] K. Padiyar and A. Kulkarni, "Control design and simulation of unified power flow controller," *IEEE Trans. Power Del.*, vol. 13, no. 4, pp. 1348–1354, Oct. 1998.

[5] *EMTDC User's Guide*. Winnipeg, MB, Canada: Manitoba HVDC Research Center, 2010.

[6] S. Filizadeh, A. Gole, D. A. Woodford, and G. D. Irwin, "An optimization-enabled electromagnetic transient simulation-based methodology for hvdc controller design," *IEEE Trans. Power Del.*, vol. 22, no. 4, pp. 2559–2566, Oct. 2007.

[7] A. Ghosh, G. Ledwich, O. P. Malik, and G. S. Hope, "Power system stabilizer based on adaptive control techniques," *IEEE Trans. Power App. Syst*, vol. PAS-103, no. 8, pp. 1983–1989, Aug. 1984.

[8] O. P. Malik, G. P. Chen, G. S. Hope, Y. H. Qin, and G. Y. Xu, "Adaptive self-optimising pole shifting control algorithm," *Proc. Inst. Elect. Eng., Control Theory Appl*, vol. 139, no. 5, pp. 429–438, 1992.

[9] R. Gokaraju and O. P. Malik, "Radial basis function identifier and pole-shifting controller for power system stabilizer applicat," *IEEE Trans. Energy Convers.*, vol. 19, no. 4, pp. 663–670, Dec. 2004.

[10] K. J.Åström and B. Wittenmark, *Adaptive Control*, 2nd ed. New York: Dover, 2008.

[11] S. Haykin, *Adaptive Filter Theory*, T.Kailath, Ed., 4th ed. Upper Saddle River: Prentice-Hall, 2001.

[12] Q. H. Wu and B. W. Hogg, "Robust self-tuning regulator for a synchronous generator," *Proc. Inst. Elect. Eng., Control Theory Appl.*, vol. 135, no. 6, pp. 463–473, 1988.

[13] A. Rahim, E. Nowicki, and O. Malik, "Enhancement of power system dynamic performance through an on-line self-tuning adaptive svc controller," *Elect. Power Syst. Res*, vol. 76, no. 9-10, pp. 801–807, 2006.

[14] R. Sadikovic, P. Korba, and G. Andersson, "Self-tuning controller for damping of power system oscillations with facts devices," presented at the IEEE Power Eng. Soc. Gen. Meeting, Montreal, QC, Canada, 2006.

[15] A. Domahidi, B. Chaudhuri, P. Korba, R. Majumder, and T. C. Green, "Self-tuning flexible AC transmission system controllers for power oscillation damping: a case study in real time," *IET Gen., Transm. Distrib.*, vol. 3, no. 12, pp. 1079–1089, 2009.

[16] P. Korba, M. Larsson, B. Chaudhuri, B. Pal, R. Majumder, R. Sadikovic, and G. Andersson, "Towards real-time implementation of adaptive damping controllers for facts devices," in *Proc. IEEE Power Eng. Soc. Gen. Meeting*, 2007, pp. 1–6.

[17] S. J. Cheng, O. P. Malik, and G. S. Hope, "Damping of multi-modal oscillations in power systems using a dual-rate adaptive stabilizer," *IEEE Trans. Power Syst.*, vol. 3, no. 1, pp. 101–108, Feb. 1988.
[18] G. P. Chen and O. P. Malik, "Tracking constrained adaptive power system stabiliser," *Proc. Inst. Elect. Eng., Gen., Transm. Distrib.*, vol. 142, no. 2, pp. 149–156, 1995.
[19] P. C. Krause, O. Wasynczuk, and S. D. Sudhoff, *Analysis of Electric Machinery and Drive Syst*, 2nd ed. Hoboken, NJ, USA: Wiley, 2002.
[20] N. G. Hingorani, *Understanding FACTS: concepts and technology of flexible AC transmission syst*, L.Gyugyi, Ed. Piscataway, NJ, USA: IEEE, 2000.
[21] S. Jiang, U. Annakkage, and A. Gole, "A platform for validation of facts models," *IEEE Trans. Power Del.*, vol. 21, no. 1, pp. 484–491, Jan. 2006.
[22] L.Ängquist and C. Gama, "Damping algorithm based on phasor estimation," in *Proc. IEEE Power Eng. Soc. Winter Meeting*, 2001, vol. 3, pp. 1160–1165.
[23] D. J. Trudnowski, J. M. Johnson, and J. F. Hauer, "Making Prony analysis more accurate using multiple signals," *IEEE Trans. Power Syst*, vol. 14, no. 1, pp. 226–231, Feb. 1999.

Dipendra Rai (S'07-M'13) received the B.E. degree in electrical engineering from Tribhuvan University (T.U.), Nepal, in 2004 and the M.Sc. and Ph.D. degrees in electrical engineering from the University of Saskatchewan, Saskatoon, SK, Canada, in 2008 and 2012, respectively.

Currently, he is a System Planning Engineer at BC Hydro, Vancouver, BC, Canada. His research interests include flexible ac transmission system controllers and power systems dynamics.

Ramakrishna Gokaraju (S'88–M'00) received the M.Sc. and Ph.D. degrees in electrical and computer engineering from the University of Calgary, Calgary, AB, Canada, in 1996 and 2000, respectively.

During 1992–1994, he was a Graduate Engineer with Larsen & Toubro-ECC, Madras, India; a Research Engineer with Regional Engineering College, Rourkela, India; and a Project Associate with the Indian Institute of Technology, Kanpur, India. During the period 1999 to 2002, he was with the Alberta Research Council as a Research Scientist and the IBM Toronto Lab as a Staff Software Engineer. He joined the University of Saskatchewan, Saskatoon, SK, Canada, in 2003 and is presently an Associate Professor. He is a registered professional engineer in the Province of Saskatchewan. His current research work is in power systems protection and control, real time simulations, and smart grids.

Sherif O. Faried (S'88–M'88–SM'00) received the B.Sc. and M.Sc. degrees in electrical engineering from Ain Shams University, Cairo, Egypt, in 1979 and 1984, respectively, and the M.Sc. and Ph.D. degrees in electrical engineering from the University of Saskatchewan, Saskatoon, SK, Canada, in 1988 and 1993, respectively.

Currently, he is a Professor of Electrical Engineering in the Department of Electrical and Computer Engineering, University of Saskatchewan. He is a Registered Professional Engineer in the Province of Saskatchewan.